Draft Manuscript for Review

An analytical model for the dynamic stiffness of a dowel-type timber connection

Journal:	*Holz als Roh- und Werkstoff*
Manuscript ID:	Draft
Manuscript Type:	ORIGINALARBEITEN / ORIGINALS
Date Submitted by the Author:	n/a
Complete List of Authors:	Reynolds, Thomas; University of Bath, Architecture and Civil Engineering Harris, Richard; University of Bath, Architecture and Civil Engineering Chang, Wen-Shao; University of Bath, Architecture and Civil Engineering
Keywords:	timber, dynamics, connections, dowel, stress function, foundation modulus, vibration, serviceability

Note: The following files were submitted by the author for peer review, but cannot be converted to PDF. You must view these files (e.g. movies) online.

Analytical.tex
References.bib
spbasic.bst
svglov3.clo
svjour3.cls

European Journal of Wood and Wood Products manuscript No.
(will be inserted by the editor)

An analytical model for the dynamic stiffness of a dowel-type timber connection

Thomas Reynolds · Richard Harris · Wen-Shao Chang

Received: date / Accepted: date

Abstract The dynamic stiffness of dowel-type connections for timber structures is investigated. The fundamental part of a dowel-type connection is the embedment of a steel dowel into the timber that surrounds it, and the stiffness of the timber in embedment is represented by the foundation modulus. A standard experimental method for identifying the foundation modulus under static load is modified to assess the secant stiffness exhibited under one-sided small-amplitude vibration. It is shown that the steady-state dynamic stiffness is significantly higher than the static stiffness for under initial loading, and that, if the amplitude of vibration is sufficiently small, a simple analytical elastic model predicts the foundation modulus well. The analytical model is based on a complex stress function for the timber in embedment, and the frictional interaction between the dowel and the timber. The foundation modulus calculated in this way can be used to predict the stiffness of complete connections for analysis of frames modelled with semi-rigid joints. Although the application of the model is limited to vibration about a non-zero mean load, with no load-sign reversal, this form of vibration encompasses various important types of in-service vibration of structures, such as that induced by turbulent wind or footfall.

Keywords timber · dynamics · connections · dowel-type · embedment · foundation modulus · vibration · serviceability · analytical model · stress function

T. Reynolds · R. Harris · W. Chang
University of Bath, Claverton Down, Bath BA2 7AY UK
Tel.: +44(0)1225385943
Fax: +44(0)1225386691
E-mail: tpsr20@bath.ac.uk

1 Introduction

Wind, footfall and machinery can cause vibration in structures. Vibration above a certain level may be perceived by occupants or users of the structure, and this can lead to complaint. While such vibration may not necessarily cause structural damage, complaint by users represents a serviceability failure, which may result in additional costs in modifying the structure to perform appropriately, and may also reduce public confidence in a particular form of construction. Such phenomena are magnified by the light weight and flexibility of timber and engineered timber products, when compared to alternative structural materials.

In order to reduce the likelihood of excessive vibration, the structural engineer must have accurate design parameters. One important parameter is the dynamic stiffness exhibited by the system.

To predict the behaviour of a structure, the stiffness properties of each component of the structure must be known, and the stiffness of connections can be an important factor in the design of timber structures. The foundation modulus is the stiffness, per unit length of connector, of the resistance of the timber to the embedment of a rigid dowel. It is a fundamental parameter in assessing the stiffness of dowel-type connections. Dowel-type connections are widely used, and include nails, screws, bolts and plain dowels.

In this paper, the foundation modulus applicable to vibrations has been investigated, by means of experimental work on the interaction between timber and connector under dynamic load. The dynamic stiffness in a single dowel has also been theoretically estimated based on the orthotropic elastic properties of the timber and the coefficient of friction between the steel and the timber. Material properties for the theoretical model

are obtained through tests on specimens extracted from the dynamic test pieces, and the predictions are tested against the experimental results.

This dynamic foundation modulus is based on the relative deformation of the timber around the dowel for each cycle of applied force. It differs from the static foundation modulus, which is based on the total deformation of the timber under a gradually applied force. This analytical and experimental work focusses on vibration without load sign reversal, so, throughout the cycle, a compressive force is maintained on the specimen. This is an important form of in-service vibration since it corresponds, for example, to footfall-induced vibration, where the self-weight and imposed load on the structure provides a mean force about which the footfall force induces oscillation. A similar form of vibration occurs as a result of turbulent wind load on a structure, in which the mean wind force is greater than the oscillating component caused by turbulence.

2 Background

As structural engineers strive to create more efficient structures, reducing the self-weight of floors and bridges as far as possible, serviceability criteria such as vibration become an important factor in design. There are examples of modern structures in every main construction material which have exhibited unacceptable vibration, and timber is no exception. The lateral vibration caused by footfall in the Lardal footbridge is a notable one (Inglfsson et al, 2012). Heiduschke (2008) noted that the flexibility of connections in multi-storey timber buildings means that they may experience an unacceptable amplitude of vibration under wind load, even though they may not reach the height at which buildings in conventional structural materials experience such problems.

Dowel-type connections are widely used in timber structures, and their relative flexibility means that they play an important role in the behaviour of the structure as a whole, under both static and dynamic load. Researchers have investigated the contribution of dowel-type connections to the behaviour of trusses (Larsen and Jensen, 2000), sheathed wall panels (Šilih et al, 2005) and frames with moment connections (Nishiyama and Ando, 2003). Larsen and Jensen (2000) identify the conditions under which a semi-rigid joint analysis is possible, including the tight fit of connectors to avoid unpredictable initial slip.

Experimental campaigns have been carried out to identify the force-displacement response of dowel-type connections between timber elements under cyclic loads (Foliente, 1995; Allotey and Foschi, 2004; Foschi, 2000; Heiduschke, 2006a; Noguchi and Komatsu, 2004), and the results have been used to develop models of the joints. These focus predominantly on the post-yield behaviour applicable to seismic and extreme wind events. The joint model can then be used to form part of a numerical model of a complete structure. This type of analysis can be used to assess the behaviour of existing forms of construction under dynamic loading, as was done by He (2001) and Heiduschke (2006b), or to predict the performance of proposed devices and techniques, as by Loo et al (2012) for slip-friction connectors, or by Awaludin et al (2008) for pretensioned bolts.

Small-amplitude vibration of timber structures in service differs in two ways from seismic loading: One is that neither the timber nor the steel yields, though the behaviour of the timber cannot be expected to be completely linear. The other is that the vibrations are often one-sided. That is to say, the vibrations are often small-amplitude oscillations around a non-zero mean, with no reversal of the load. This is the case for footfall-induced vibration of floors and bridges, as well as along-wind vibration of structures due to turbulent wind load. Under one-sided vibration, the dynamic stiffness of the connections is independent of the initial slip, which has already occurred, and so the condition given by Larsen and Jensen (2000) for analysis with semi-rigid joints is met.

Tests on completed timber buildings to investigate their behaviour in response to small vibrations are rare. One example, for the widely used sheathed stud wall form of construction, is Ellis and Bougard's investigation of the BRE Timber Frame 2000 building (Ellis and Bougard, 2001).

This paper seeks to provide a basis for predicting the response of timber structures with dowel-type connections to small vibrations, based on the fundamental material properties and geometry of the connection. The pre-yield behaviour of a dowel-type connector in timber is investigated by considering it as a pin-loaded orthotropic elastic plate. A complex stress function for an orthotropic plate in plane stress, with a hole loaded along its edge, was proposed by Lekhnitskii (1968). This general form of the function was adapted to the particular case in which the load on the edge of the hole is applied by a rigid circular section, referred to as a pin-loaded plate, by De Jong (1977). Different forms of the function have been developed to investigate various phenomena affecting the behaviour of the pin-loaded plate. Zhang and Ueng (1984) incorporated the effect of friction at the interface between pin and plate and Hyer and Klang (1985) allowed for deformation of the pin and clearance between the hole and the pin, as well as friction.

Despite the availability of nonlinear finite element modelling software capable of dealing with this geometry and loading, there continues to be research interest in the stress function approach, such as the development of a new form of solution by Aluko and Whitworth (2008). One reason for the enduring interest in this approach is the speed of calculation, and Derdas and Kostopoulos (2011) use the stress function to define the loading along the hole edge, and apply that loading to a finite element model, thus reducing the finite element model to a linear elastic one and avoiding the computational cost of carrying out a contact-element analysis.

The potential for application of this method to timber has been clear since Lekhnitskii (1968) used the material properties for plywood in the example calculations in his book. The further research described above was, however, generally motivated by the use of pin-jointed composites in aircraft and it was Echavarra et al (2007) who noted its potential for application to dowel-type connections in timber structures, and developed a particular form of the stress function for that purpose.

All of the above researchers used the complex stress function approach as a tool for analysis of the stress distribution around the pin. Since the stress function defines the strain field in the plate, it can also be used to consider deformation of the connection, and it is on that aspect that this research focusses.

Sjödin et al (2006) measured the strain field in the timber around a group of dowels, and showed that an elastic orthotropic plane-stress model for the timber could accurately represent the strain distribution. The same researchers then showed the influence of friction between the dowel and the timber on that strain distribution (Sjödin et al, 2008).

This research presents and tests a model in the form of an analytical set of equations which takes into account the interface friction and the orthotropy of the timber.

3 Material and methods

3.1 Analytical method

The load-deflection response of a circular dowel embedding into a piece of timber depends on the orthotropic elastic behaviour of the timber, and also on the frictional interaction between the dowel and the timber. The deformation of the cross-section of the steel dowel is assumed to be negligible, but the friction between the steel and timber determines the distribution of the forces around the face of the timber, so must be modelled.

This method has been developed on the assumption

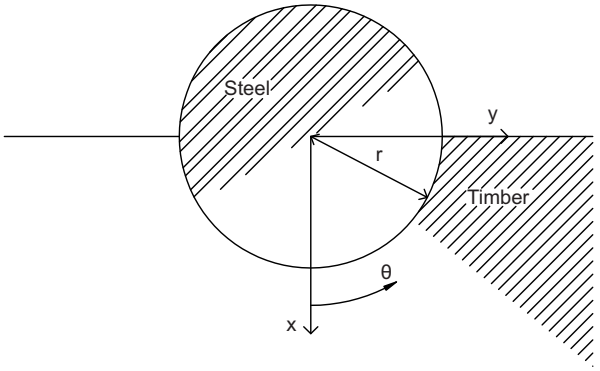

Fig. 1 Geometry for analysis

that, under small-amplitude vibration significantly below the embedment strength, the behaviour of the timber can be treated as linear, and therefore modelled using an orthotropic linear elastic model. The appropriateness of this assumption is discussed later in this paper, with reference to the experimental results.

In the model, the foundation modulus for the timber is estimated using a stress function of the form first proposed by Lekhnitskii (1968), and, in particular, as derived by Zhang and Ueng (1984). The definition of the stress function exactly follows the work of these researchers, and the formulae are collated and reproduced in this paper for convenience. The work of these researchers is then extended to assess the deformations in a specimen by superposition of two semi-infinite plate solutions.

The stress function represents the stresses in a semi-infinite orthotropic plate with a half-hole in the surface. The forces applied by the dowel along the surface of the half-hole are defined on the basis of the geometry and the coefficient of friction between the steel and the timber. The geometry and notation are shown in Fig. 1.

3.1.1 General form of stress function

Lekhnitskii (1968) showed that the general form of the stress functions for an infinite orthotropic plate with a hole is as given by (1) to (5). The solution of a particular problem relies on finding the coefficients a_n and b_n which correspond to the distribution of the load on the edge of the hole. $\zeta_{1,2}$ are transformed coordinates describing the point on the plate under consideration. The complex stress functions and Φ_1 and Φ_2 are defined so that the displacements u and v are given by (6) and (7). i is the imaginary unit.

$$\Phi_1 = a_0 ln\zeta_1 + \sum_{n=2}^{\infty} \frac{a_n}{\zeta_{1,n}} \quad (1)$$

$$\Phi_2 = b_0 ln\zeta_2 + \sum_{n=2}^{\infty} \frac{b_n}{\zeta_{2,n}} \tag{2}$$

$$\zeta_1 = \frac{z_1 + \sqrt{z_1^2 - (1+\mu_1^2)}}{r^2\,(1 - i\mu_1^2)} \tag{3}$$

$$\zeta_2 = \frac{z_2 + \sqrt{z_2^2 - (1+\mu_2^2)}}{r^2\,(1 - i\mu_2^2)} \tag{4}$$

$$z_1 = x + \mu_1 y \quad z_2 = x + \mu_2 y \tag{5}$$

$$u = 2\mathrm{Re}\,(p_1\Phi_1 + p_2\Phi_2) + U \tag{6}$$

$$v = 2\mathrm{Re}\,(q_1\Phi_1 + q_2\Phi_2) \tag{7}$$

$Re\,()$ denotes the real part of what is, in general, a complex number in the brackets. u is the displacement relative to a particular fixed point, and includes one non-zero constant of integration, U. μ_1, μ_2, p_1, p_2, q_1 and q_2 are derived from the material properties of the plate material, the timber, as in (8) to (13), where E_1 is the elastic modulus of the plate material in the x direction, E_2 the elastic modulus in the y direction, G is the shear modulus, and ν_1 the Poisson's ratio.

$$\mu_1^2 = \frac{2\nu_1 - \frac{E_1}{G} + \sqrt{\left(2\nu_1 - \frac{E_1}{G}\right)^2 - \frac{4E_1}{E_2}}}{2} \tag{8}$$

$$\mu_2^2 = \frac{2\nu_1 - \frac{E_1}{G} - \sqrt{\left(2\nu_1 - \frac{E_1}{G}\right)^2 - \frac{4E_1}{E_2}}}{2} \tag{9}$$

$$p_1 = \frac{\mu_1^2}{E1} - \frac{\nu_1}{E_1} \tag{10}$$

$$p_2 = \frac{\mu_2^2}{E1} - \frac{\nu_1}{E_1} \tag{11}$$

$$q_1 = \frac{1}{\mu_1 E_2} - \frac{\nu_1\mu_1}{E_1} \tag{12}$$

$$q_2 = \frac{1}{\mu_2 E_2} - \frac{\nu_1\mu_2}{E_1} \tag{13}$$

Lekhnitskii (1968) presents a method to allow the stress functions to be defined on the basis of the trigonometric series defining the displacements u' and v' on the hole edge. The general form of those series is as in (14) and (15). $\sigma = e^{i\theta}$. α_m and β_m are coefficients determined by the boundary conditions and $*$ denotes the complex conjugate.

$$u' = \alpha_0 + \sum_{m=1}^{\infty} \left(\alpha_m\sigma^m + \alpha_m^*\sigma^{-m}\right) \tag{14}$$

$$v' = \beta_0 + \sum_{m=1}^{\infty} \left(\beta_m\sigma^m + \beta_m^*\sigma^{-m}\right) \tag{15}$$

Once the coefficients are determined, they can be used to generate the stress functions using (16) to (19), where $D = p_1q_2 - p_2q_1$. Note that α_0 and β_0 do not affect the stress distribution in the plate. The overall movement of the hole, caused by a net force P on the hole, is allowed for by A and B.

$$\Phi_1(z_1) = Aln\zeta_1 + \frac{(\alpha_1^*q_2 - \beta_1^*p_2)}{D\zeta_1} + \frac{1}{D}\sum_{m=2}^{\infty}(\alpha_m^*q_2 - \beta_m^*p_2)\,\zeta_1^{-m} \tag{16}$$

$$\Phi_2(z_2) = Bln\zeta_2 + \frac{(\alpha_1^*q_1 - \beta_1^*p_1)}{D\zeta_2} + \frac{1}{D}\sum_{m=2}^{\infty}(\alpha_m^*q_1 - \beta_m^*p_1)\,\zeta_2^{-m} \tag{17}$$

$$A = \frac{P}{\pi i}\left(\frac{\mu_1\mu_1^* + \mu_1\mu_2^* - \frac{a_{12}}{a_{22}}\mu_1\mu_2\mu_1^*\mu_2^*}{(\mu_1 - \mu_1^*)(\mu_1 - \mu_2)(\mu_1 - \mu_2^*)}\right) \tag{18}$$

$$B = \frac{P}{\pi i}\left(\frac{\mu_2\mu_2^* + \mu_2\mu_1^* - \frac{a_{12}}{a_{22}}\mu_2\mu_1\mu_2^*\mu_1^*}{(\mu_2 - \mu_2^*)(\mu_2 - \mu_1)(\mu_2 - \mu_1^*)}\right) \tag{19}$$

3.1.2 Boundary conditions

Zhang and Ueng (1984) used the displacement boundary conditions described in (20) to (22), for the geometry shown in Fig. 1, to define the stress functions. In doing so, they assumed that the dowel remained rigidly circular, so that the radial displacement of the timber equals that of the face of the dowel, and that some slip occurs in the tangential direction, at all points except $\theta = 0$.

$$u = \frac{u_0}{c} \quad \text{and} \quad v = 0 \quad \text{when} \quad \theta = \pm\frac{\pi}{2} \tag{20}$$

$$u = u_0 \quad \text{and} \quad v = 0 \quad \text{when} \quad \theta = 0 \tag{21}$$

$$(u_0 - u)\cos\theta = v\sin\theta \quad \text{when} \quad \frac{-\pi}{2} \le \theta \le \frac{\pi}{2} \tag{22}$$

u_0 is, therefore, the displacement of the dowel in the semi-infinite plate, and c represents the extent to which the dowel slips along the surface of the timber. Zhang and Ueng (1984) proposed the trigonometric series in (23) to (31) to satisfy these boundary conditions. Using these boundary conditions, the standard form of stress function defined by (14) and (15), the stress functions for this particular case are defined as in (32) and (33).

$$u' = \frac{c-1}{2c}u_0\cos 2\theta + \frac{c+1}{2c}u_0 cos4\theta \tag{23}$$

$$v' = \left(\frac{c-1}{2c} + \frac{c+1}{c}\right)u_0\sin 2\theta + \frac{c+1}{2c}u_0 sin4\theta \tag{24}$$

$$c = \frac{B_1 - A_1}{A_1} \tag{25}$$

$$u_0 = \frac{gP}{\pi}\frac{(B_1 - A_1)}{2A_1(\nu_1 - k - nk) - B_1(\nu_1 - k - nk)} \tag{26}$$

$$A_1 = (19n + 11nk + 10k - 10\nu_1) + \mu\,(11n - 6nk + 15k - 15\nu_1) \quad (27)$$

$$B_1 = 10n\,(1-k) + 10\mu\,(3k - 3\nu_1 + 2nk + n) \quad (28)$$

$$k = \sqrt{\frac{E_1}{E_2}} \quad (29)$$

$$n = \sqrt{2\,(k-\nu_1) + \frac{E1}{G}} \quad (30)$$

$$g = \frac{1-\nu_1\nu_2}{E2} + \frac{k}{G} \quad (31)$$

$$\Phi_1 = A \ln\zeta_1 + \left(\frac{c-1}{2x}\frac{q_2 - ip_2}{2D} - \frac{c+1}{c}\frac{ip_2}{2D}\right)\frac{u_0}{\zeta_1^2} + \frac{c+1}{2c}\frac{q_2 - ip_2}{2D}\frac{u_0}{\zeta_1^4} \quad (32)$$

$$\Phi_2 = B \ln\zeta_2 + \left(\frac{-(c-1)}{2x}\frac{q_1 - ip_1}{2D} + \frac{c+1}{c}\frac{ip_1}{2D}\right)\frac{u_0}{\zeta_2^2} - \frac{c+1}{2c}\frac{q_1 - ip_1}{2D}\frac{u_0}{\zeta_2^4} \quad (33)$$

Although the general solution by Lekhnitskii (1968) is for a hole in an infinite plate, the form of the stress functions proposed by Zhang and Ueng (1984) means that the vertical component of the resultant force applied to the plate is zero on the y axis. These functions therefore approximate a semi-infinite plate with a half-hole, which is appropriate for the geometry in the experimental work described in Section 3.2.

It should be noted that this is only an approximate solution for a semi-infinite plate with a half-hole, because the shear stress on the y axis is not zero. Zhang and Ueng (1984) show that this approximation does not affect the stress field significantly, and it is therefore assumed that it will not significantly affect the vertical deformations.

3.1.3 Superposition for displacements

The deformation of the dowel for a particular applied load, and particular support conditions, will, in general, be different from the deformation u_0. The strain field is integrated to give the deformations in the plate, resulting, for this case, in one non-zero constant of integration, U in (23). In this paper, the constant is eliminated by superimposing the solutions for two holes loaded in opposite directions. By placing the second $2h$ below the first, as shown in Fig. 2, a line of zero displacement is created at a vertical distance h from the hole. If the holes are sufficiently well separated that there is no significant interaction between the stresses on the edges of each hole, then this is a reasonable representation of a plate supported rigidly along one edge.

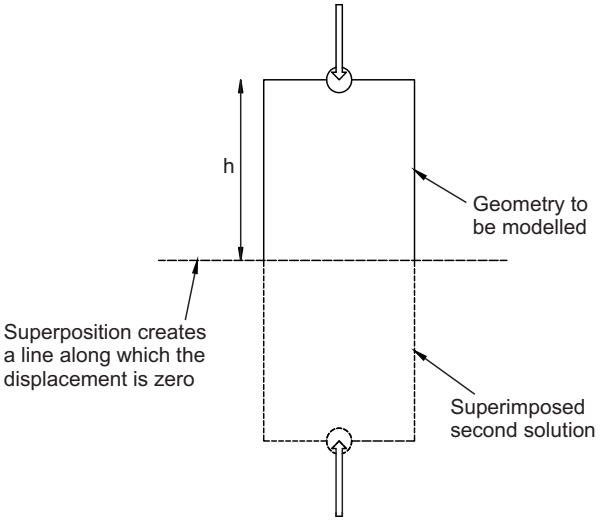

Fig. 2 Superposition of two infinite-plate solutions to model a supported edge

In order to calculate the movement of the dowel, the displacement of the timber in the semi-infinite plate is calculated in two positions, u_0 at $y = 0$, $x = r$ and u_1 at $y = 0$, $x = 2h - r$. u_0 can be calculated directly using (26). For u_1, the transformed coordinates ζ_1 and ζ_2 are calculated using (3) and (4). Since the point is on the x-axis, ζ_1 and ζ_2 are equal in both cases. Φ_1 and Φ_2 are then calculated using (32) and (33), for a unit applied force P. u_1 is then calculated using (6).

The displacement of the dowel relative to the fixed surface at $x = h$ is then given by $\frac{u_1 - u_0}{2}$, and the predicted stiffness of the specimen can be calculated as $\frac{2}{u_1 - u_0}$.

3.2 Experimental method

The experimental testing consisted of three parts. First, the foundation modulus of the timber under dynamic loading was found. Then the parameters required for the analytical determination of the foundation modulus were investigated: The frictional resistance of the dowel in a half-hole and the elastic moduli of the timber in each grain orientation. The timber used was Douglas fir grown in the United Kingdom, which was stored for 12 weeks after delivery in a controlled environment, with the temperature maintained at $18 - 22°$C, and relative humidity at $60 - 65\%$.

3.2.1 Foundation modulus

The experimental method is based on the static test method described in ASTM D5764 (ASTM, 1997). This method uses a piece of timber with a half-hole in its surface. In contrast, methods such as the European

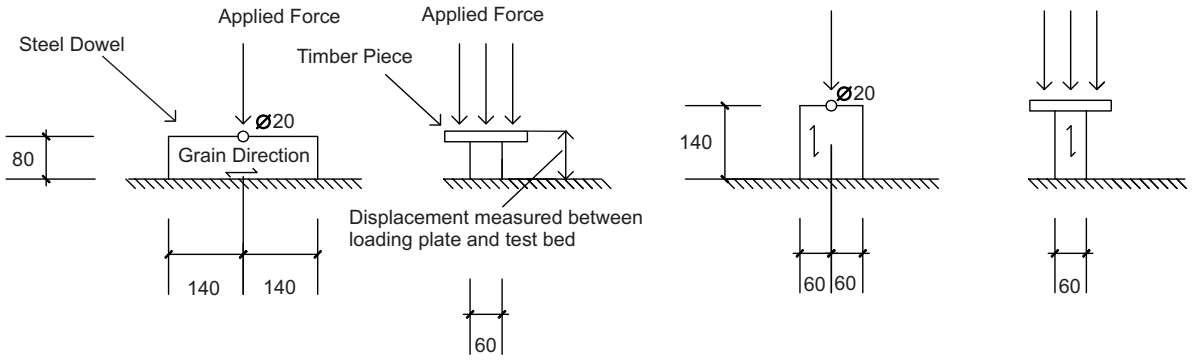

Fig. 3 Schematic diagram of test setup with perpendicular-to-grain (left) and parallel-to-grain (right) specimens (dimensions in mm)

Norm EN 383 (BSI, 2007) use a piece with a complete hole through the centre. Using a timber piece with a half-hole enables the dowel to be held rigidly straight, which means that the displacement of the dowel is uniform along its length, and the displacement of the loading head is an accurate measure of the deformation of the timber. This is particularly important given the high stiffness of the timber under dynamic loading, and the correspondingly small deformations that need to be measured in these dynamic tests.

A linear variable differential transformer (LVDT) was used to measure the displacement of the loading head, except when its 2mm range was exceeded; in which case, the built-in displacement transducer in the servo-hydraulic loading machine was used. Fig. 3 schematically shows the test setup and specimen dimensions for parallel- and perpendicular-to-grain specimens.

3.2.2 Static tests

In order to characterize the forces applied to the dynamic test specimens, their embedment strength was predicted according to Eurocode 5 (BSI, 2009), based on their density. The average density of 27 of the specimens was measured as 485kg/m^3, and the average moisture content of three preliminary specimens was obtained by the oven dry method according to BS EN 13183 (BSI, 2002) , and found to be 14.92%. On this basis, the adjusted density for the reference value of 12% moisture content, used in Eurocode 5, was calculated as 453kg/m^3. After the dynamic tests had been carried out, 8 of the dynamic test specimens were used for moisture content evaluation. The average moisture content was 14.57%, with a coefficient of variation of 0.065. The preliminary moisture content measurement was, therefore, considered sufficiently accurate for estimation of load capacity.

The calculated embedment strength is shown in Table 1. Four static tests were also carried out, two in each grain orientation, to verify the calculated value. The average of those results is also shown in Table 1. Since it would be the calculated value that would be used to design a connection in practice, the calculated embedment strength was used as the reference value for the forces applied in the dynamic tests.

Table 1 Embedment strength of specimens

Grain Orientation	Calculated Strength (kN)	Mean Measured Strength (kN)
Parallel	35.7	33.9
Perpendicular	21.6	17.7

3.2.3 Dynamic tests

Each specimen was subjected to 1000 sinusoidal cycles of force at 1Hz. The peak force was either 20%, 40% or 80% of the calculated embedment strength of the specimen. The amplitude of the sinusoid was given by the R-ratio, as defined by (34), where F_{peak} is the maximum compressive force in the cycle, and F_{trough} is the minimum compressive force. Nominal R-ratios of 1.2 and 10 were tested.

$$R = \frac{F_{peak}}{F_{trough}} \tag{34}$$

Each combination of grain orientation, peak force and R-ratio was tested, resulting in a total of 12 tests, as shown in Table 2. There were three repetitions of each, giving 36 specimens in total. The steady-state values of secant stiffness were assessed for comparison with the results of the analytical model. The secant stiffness is taken as the slope on the force-displacement diagram between the points of maximum and minimum displacement in each 1 second period, as shown in Fig. 4.

Table 2 Summary of dynamic tests

Test No.	Grain Orientation	Peak Force F_{peak} (% of Static Failure Stress)	R ratio $\frac{F_{peak}}{F_{trough}}$
1	Parallel	20%	1.2
2	Parallel	20%	10
3	Parallel	40%	1.2
4	Parallel	40%	10
5	Parallel	80%	1.2
6	Parallel	80%	10
7	Perpendicular	20%	1.2
8	Perpendicular	20%	10
9	Perpendicular	40%	1.2
10	Perpendicular	40%	10
11	Perpendicular	80%	1.2
12	Perpendicular	80%	10

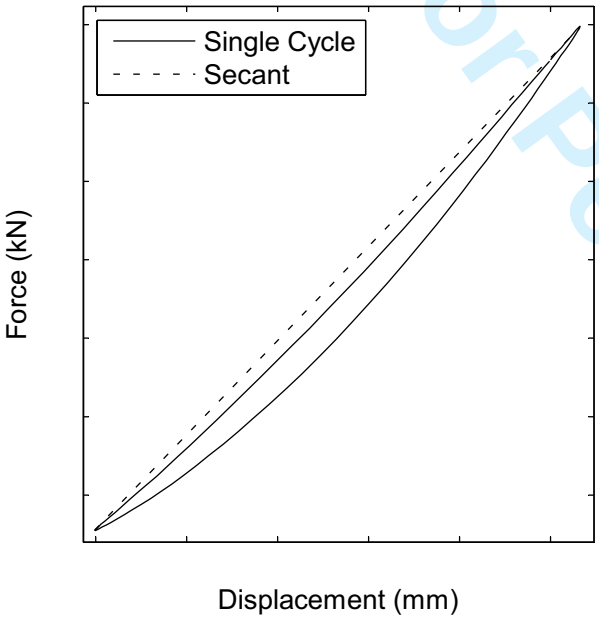

Fig. 4 Secant stiffness

3.2.4 Friction tests

Tests were carried out to estimate the coefficient of friction to use in the analytical model. Fig. 5 shows the test setup, in which a vertical force was applied to two specimens, with a long dowel between. The vertical load was applied by a servo-hydraulic loading machine, which allowed the load to be held constant despite any vertical settlement. The dowel was pushed horizontally using a hydraulic hand jack, and the force required to do so was continuously recorded through a load cell.

It should be noted that the friction force in this test setup is in a different orientation to the friction force developed during embedment of the dowel into the timber. Tests by McKenzie and Karpovich (1968) showed

Fig. 5 Friction test on dynamic test specimens

that the grain orientation had no significant effect on the magnitude of either the static or steady sliding friction coefficients. It is considered reasonable, therefore, to assume that the frictional behaviour will be similar in both orientations, so that this test provides a suitable estimate of the coefficient of friction for use in the analytical model.

Three tests were carried out with the load parallel to the grain, and three with the load perpendicular to the grain, using pairs of specimens with the same dimensions as those used for dynamic tests.

3.2.5 Elastic moduli

The principal elastic moduli were determined from tests on specimens extracted from some of the dynamic test specimens, following the method given in BS EN 408 (BSI, 2011). The specimens for which elastic modulus data were obtained are summarized in Table 3. Two elastic modulus specimens were taken from each dynamic test specimen, one in each grain direction, so 26 elastic moduli were obtained in each grain direction, 52 in total.

4 Results

4.1 Experimental results

4.1.1 Secant stiffness

The measured stiffness was not constant throughout each test. Fig. 6 shows the variation of stiffness through the test for a typical specimen, in which each point represents the measured secant stiffness for one of the 1000 cycles of force applied. The stiffness was observed to increase, with the rate of increase reducing throughout the test. For the test shown in Fig. 6, the stiffness had reached a fairly constant value beyond approximately

Table 3 Dynamic test specimens from which elastic modulus specimens were extracted

Test	Grain Orientation	Peak Force F_{peak} (% of Static Failure)	R-ratio $\frac{F_{peak}}{F_{trough}}$	No. of Specimens
1	Parallel	20%	1.2	2
2	Parallel	20%	10	2
3	Parallel	40%	1.2	3
4	Parallel	40%	10	2
5	Parallel	80%	1.2	3
6	Parallel	80%	10	1
7	Perpendicular	20%	1.2	3
8	Perpendicular	20%	10	2
9	Perpendicular	40%	1.2	2
10	Perpendicular	40%	10	2
11	Perpendicular	80%	1.2	2
12	Perpendicular	80%	10	2

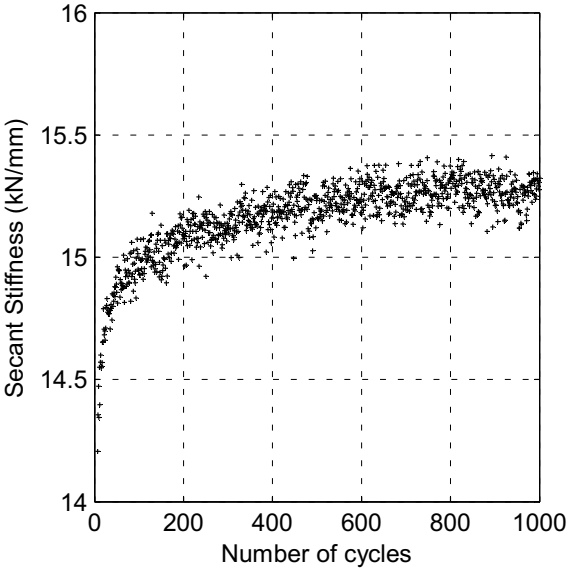

Fig. 6 Variation of stiffness for a peak force of 40% of the embedment strength, $R = 10$, perpendicular to grain

the 700th cycle, and this was typical.

Some parallel-to-grain specimens tested at $R = 1.2$, however, still exhibited a significant rise in stiffness at the end of the test, and the most extreme case is shown in Fig. 7. The specimen therefore failed to reach a steady-state value of stiffness during the test. This had consequences for the comparison of these experimental results with analytical predictions, as discussed in Section 4.3.

The surface of the timber in contact with the steel will not have been perfectly smooth and tight fitting, due to the drilling process and the heterogeneous microstructure of the timber. Part of this unevenness and lack of fit may have been gradually taken up under the applied

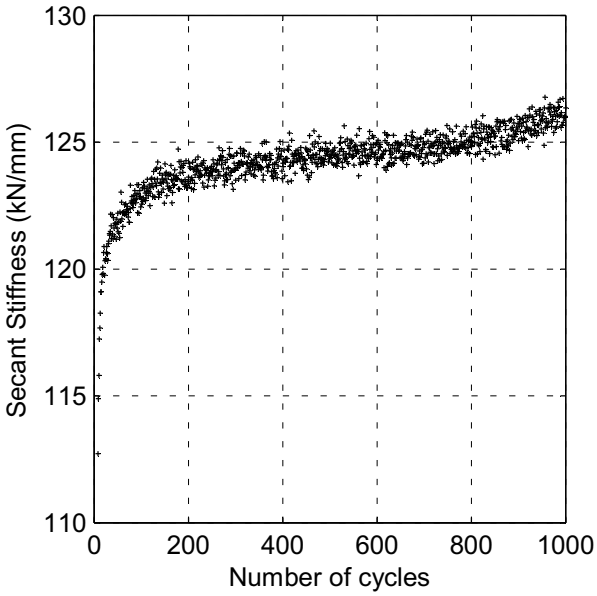

Fig. 7 Variation of stiffness for a peak force of 40% of the embedment strength, $R = 1.2$, parallel to grain

force, so continually increasing the stiffness towards the value of the tight-fitting case.

The scatter in the calculated values of stiffness is thought to be due to a combination of two effects. One is that the finite sampling rate meant that the highest and lowest values of force and displacement in each cycle were not necessarily sampled. The other is that electrical noise in the force and displacement measurements would add a random component to each measurement, and, therefore, to the calculated stiffness. The scatter is, therefore, thought to be due to the measurement process and not indicative of the real behaviour of the specimen.

4.1.2 Effect of amplitude

Fig. 8 and Fig. 9 show the comparison of two force-displacement diagrams recorded for individual cycles of force on the same specimen. In this case, an oscillating force at $R = 10$ was applied for 200 cycles after 1000 cycles at $R = 1.2$ had been completed, so each graph is for the same specimen. It can be seen that the secant stiffness is lower for the higher-amplitude cycle at $R = 10$. This reduction in stiffness is caused by nonlinear behaviour under low forces. In fact, the force-displacement diagram for $R = 10$ shows significant nonlinear behaviour and hysteresis, while the behaviour at $R = 1.2$ is near linear.

It is thought that unevenness in the contact surface between timber and steel or lack of fit between the dowel and the hole may be taken up by the pressure on this surface, causing the behaviour to become more linear

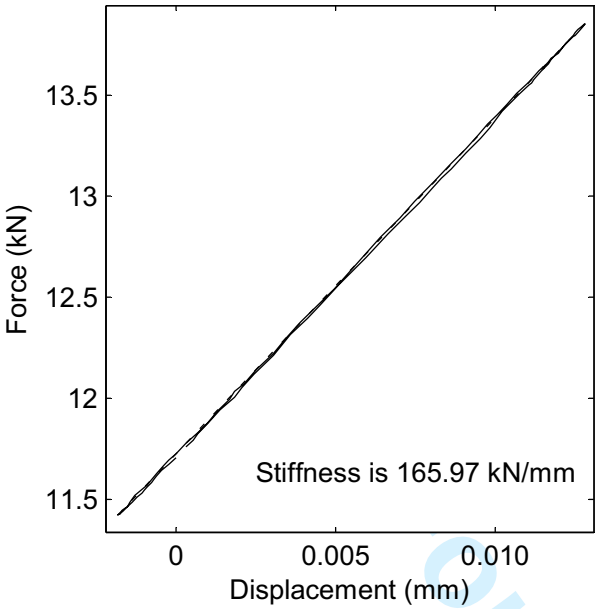

Fig. 8 Secant stiffness for a peak force of 40% of the yield force, $R = 1.2$

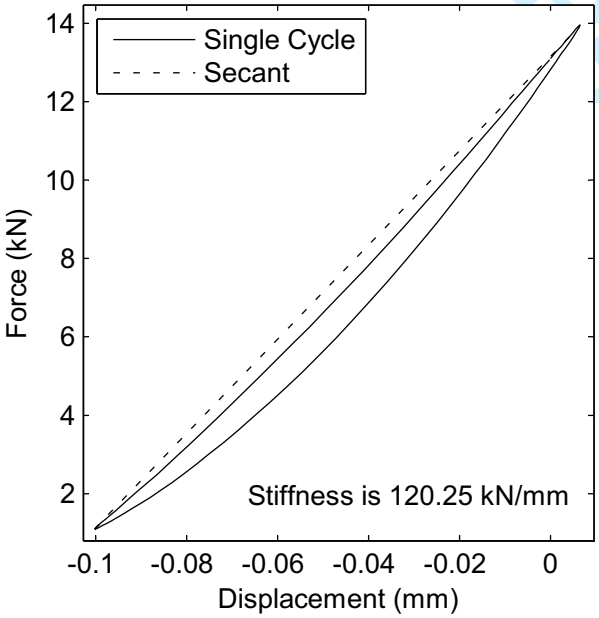

Fig. 9 Secant stiffness for a peak force of 40% of the yield force, $R = 10$

with higher forces. When the force is removed, in the $R = 10$ case, the effect of unevenness and lack of fit may be seen again at the lower loads, causing a reduction in stiffness.

4.1.3 Collated results

In order to obtain a steady-state value of stiffness for comparison between the tests, the mean of the stiffness for each cycle after the 700th was used. These stiffnesses

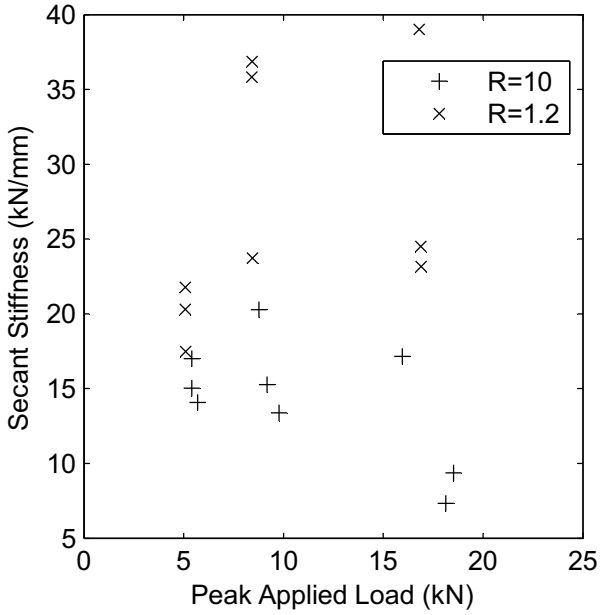

Fig. 10 Mean secant stiffness for perpendicular to grain tests

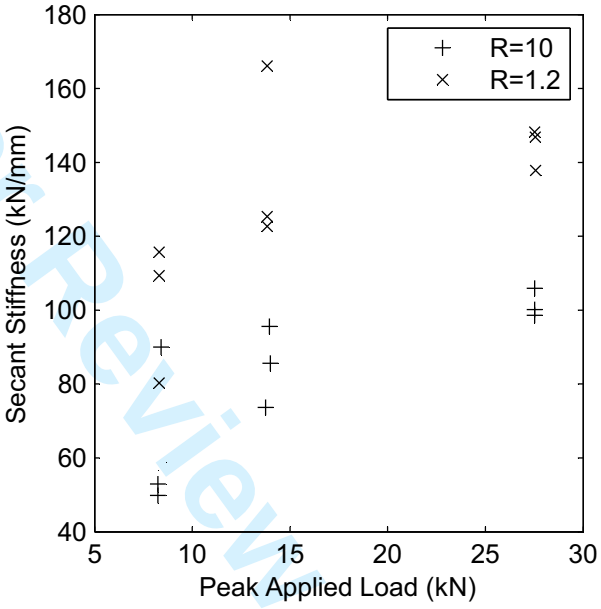

Fig. 11 Mean secant stiffness for parallel to grain tests

are plotted against the peak applied force in Fig. 10 and Fig. 11. The figures show that the peak applied force varied between repetitions of the same test, particularly in tests with a high peak load or a high amplitude of the load. This was because of the limited gain in the servo-hydraulic loading machine and the variability in specimen stiffness.

Where $R = 10$ in both the parallel- and perpendicular-to-grain tests, it can be seen that the stiffness is generally lower than the corresponding tests with $R = 1.2$. This is due to the effect of nonlinearity at low force, as described in the Section 4.1.2.

There is a large scatter of stiffnesses in all the tests, but particularly in the perpendicular-to-grain tests. This was assumed to reflect the variation of material properties in the timber, and this assumption was tested by comparing these measured values of stiffness with predictions based on the material properties of the timber in the specimens and the coefficient of friction between the dowel and the timber, as described in Section 4.2.
In each of the three tests parallel to the grain, with a peak force of 80% of the embedment strength and $R = 1.2$, the displacement sensor was not correctly positioned for the first 1000 cycles of force applied, so the results shown are for a second set of 1000 cycles.

4.1.4 Friction tests

Six friction tests were carried out: three with the load applied parallel to the grain, and three with the load applied perpendicular to the grain. Fig. 12 shows the plot of applied lateral force against lateral displacement for one of the friction tests. This highlights the influence of the rate of movement of the dowel. In part A of Fig. 12, the lever of the hand jack was pushed down slowly, which meant that the applied force dropped away before the constant rate of displacement, required for kinetic friction, could develop. The dowel therefore moved a short distance each time and then stopped, a phenomenon known as stick-slip oscillation.
In part B of Fig. 12, the lever of the hand jack was moved sufficiently quickly that kinetic friction could develop, after overcoming the initial, higher force of static friction. Since there is continuous movement in the dynamic tests, it is considered that the coefficient of kinetic friction is appropriate as the input to the analytical model. The coefficient of friction to be used in the model was therefore estimated based on the kinetic friction in each case.
In some of the parallel-to-grain friction tests, since a higher vertical load was applied, it was not possible to depress the lever of the hydraulic jack quickly enough to achieve the kinetic friction behaviour as in part B. In these cases, the lower value of force in the stick-slip oscillation, as in part A, was used to estimate the coefficient of friction. Fig. 12 shows that the lowest force measured in part A is a reasonable estimate of the coefficient of kinetic friction.
The mean ratio of the horizontal kinetic force to the vertical force for all six tests was 0.41, with a coefficient of variation of 0.1, giving an estimate of the coefficient of friction, for use in the model, of 0.21. There was no clear effect of grain orientation on the ratio of normal force to friction force.

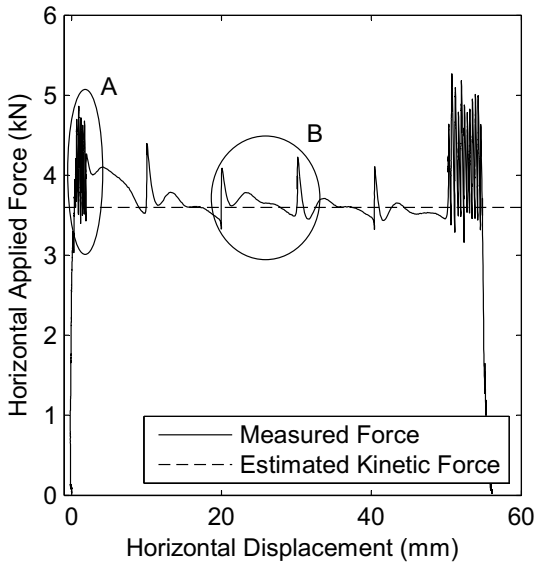

Fig. 12 Friction test results - Specimen loaded perpendicular to the grain at 8.4kN, 40% of the predicted yield force

4.1.5 Elastic modulus

The mean measured elastic modulus was $10,569\text{N/mm}^2$ in the parallel-to-grain direction, with a coefficient of variation of 0.21, and 322N/mm^2 in the perpendicular-to-grain direction, with a coefficient of variation of 0.38.

4.1.6 Estimating shear modulus

The measured values of the principal elastic moduli provided two of the four parameters required for the analytical model. In addition, the Poisson's ratio and shear modulus are required. The Wood Handbook (Forest Products Laboratory, 2010) provides mechanical properties for various species of timber, including Douglas fir. There are nine independent constants: three elastic moduli corresponding to the longitudinal, radial and tangential orientations with respect to the grain and ring structure; three shear moduli and three Poisson's ratios. The values for Douglas fir are summarized in Table 4. The mean elastic moduli from these tests were $10,569\text{N/mm}^2$ in the longitudinal direction and 322N/mm^2 in the perpendicular direction, which, for most specimens, was close to tangential. The ratio of the two moduli, was, therefore, quite different from that given in the Wood Handbook (Forest Products Laboratory, 2010). It was not, therefore, considered appropriate to obtain the shear modulus as a proportion of the longitudinal elastic modulus, using a ratio from published results. Another rationale was therefore sought to estimate the shear modulus.
Jones (1975) shows that if the elastic compliances of an

Table 4 Mechanical properties for Douglas fir, taken from the Wood Handbook (2010)

E_L (N/mm^2)	E_T (N/mm^2)	E_R (N/mm^2)	G_{LR} (N/mm^2)	G_{LT} (N/mm^2)	G_{RT} (N/mm^2)	ν_{LR}	ν_{LT}	ν_{RT}
14740	737	1002	943	1150	103	0.292	0.449	0.390

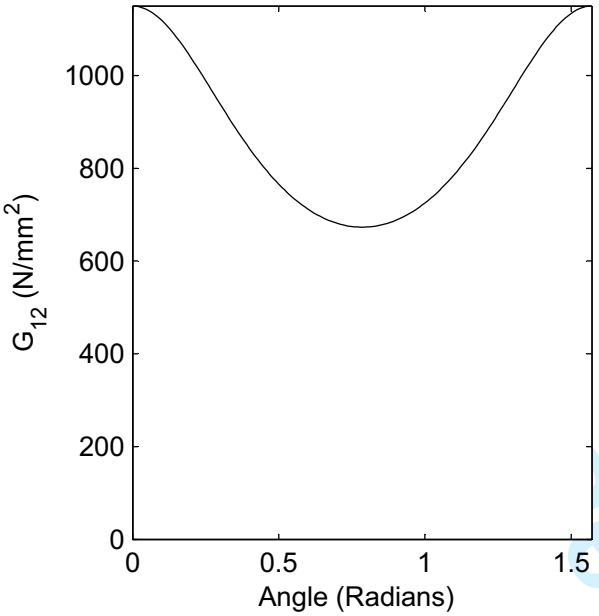

Fig. 13 Variation of apparent shear modulus with angle from the principal direction for Douglas fir

orthotropic material in plane strain are given by s_{ij}, as in (35), then the apparent shear compliance, s'_{66}, for axes at an angle θ to the principle axes, is given by (36).

$$s_{11} = \frac{1}{E_1} \quad s_{12} = \frac{-\nu_{12}}{E_1} \quad s_{22} = \frac{1}{G_{12}} \tag{35}$$

$$\begin{aligned} s'_{66} =& 4\left(s_{11} + s_{22} - 2s_{12}\right)\sin 2\theta \cos 2\theta \\ &+ s_{66}\left(\sin 2\theta - \cos 2\theta\right)^2 \end{aligned} \tag{36}$$

For Douglas fir, as described in the Wood Handbook (Forest Products Laboratory, 2010), the variation of apparent shear modulus with angle in the longitudinal-tangential plane can be plotted using (36). The result is shown in Fig. 13.

At $\theta = 45°$, s'_{66} is independent of s_{66}, and so the apparent shear modulus is independent of the principal shear modulus. Using the elastic moduli obtained from the tests, it was therefore possible to calculate the apparent shear modulus at $\theta = 45°$ for each specimen. The ratio of the maximum and minimum shear modulus from Fig. 13 was then assumed to apply to the Douglas fir used in the tests, and was used to estimate the principal shear modulus for each specimen.

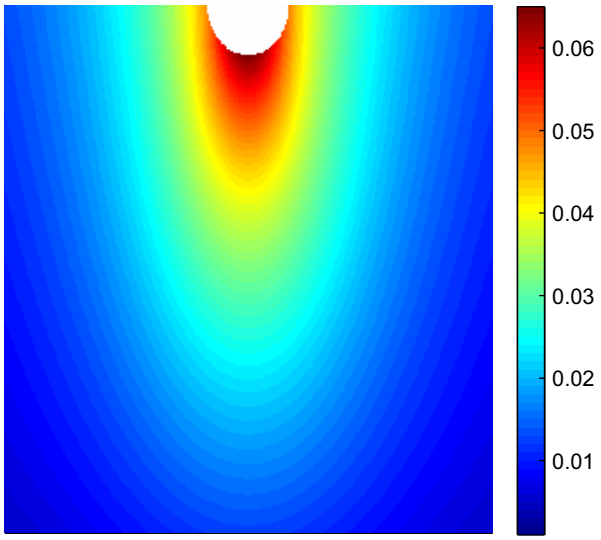

Fig. 14 Vertical displacements in mm in the timber for a typical specimen in parallel-to-grain loading (1kN applied force)

4.2 Analytical results

4.2.1 Analytical models

The two elastic moduli obtained from the tests, the Poisson's ratio for the longitudinal-tangential plane taken from the literature and the shear modulus estimated as described in the previous section were used to create a set of analytical models for the dynamic test specimens. Using these material properties and applying a unit force, the value of the two stress functions could be calculated at each point in the specimen. Using the stress functions, the displacement of every point in the specimen can be calculated. Those displacements are plotted, for illustrative purposes, in Fig. 14.

No free edge effects are allowed for on the sides of the specimen. The edge distances are considered to be sufficient that the other free edges will not significantly influence the stress or deformation fields.

4.2.2 Sensitivity to friction coefficient

The sensitivity of the analytical model to the friction coefficient was assessed by varying the coefficient between the extremes of values published by McKenzie and Karpovich (1968), from their study of friction between steel and timber. For comparison with their work,

Table 5 Effect of friction coefficient on modelled stiffness

Friction Coefficient μ	Stiffness (kN/mm)	% Change from $\mu = 0.21$
0.08	106.2	3.9%
0.21	110.5	-
0.62	120.8	9.3%

the rate of movement between the surfaces in these tests corresponds to their classification 'slow', and the surface of the steel dowel falls between his classifications of 'rough' and 'smooth'. For all the species of timber tested, the friction coefficient in these classifications ranged from 0.08 to 0.62. Using the material properties for one of the parallel-to-grain dynamic test specimens, the sensitivity analysis is summarized in Table 5, comparing these extreme values to the mean value obtained from the friction tests and used in analysis, 0.21. The resulting variation in stiffness is small in comparison to the variability in material properties in the timber. It is, therefore, considered that the sensitivity of stiffness to friction coefficient is not sufficient to justify a more extensive investigation of friction than has already been carried out.

4.2.3 Comparison with experimental results

The mean and range of analytical results was compared with the mean and range of experimental results for each grain orientation, and for each R-value. The predicted values of stiffness are independent of the magnitude of the force applied due to the assumption of elastic behaviour. The results for the three values of peak force were, therefore, combined for this comparison of predicted and measured stiffness. Fig. 15 plots the range of stiffness and the mean stiffness for the experimental results and the analytical model, with the results organized by grain orientation and R-value.

4.3 Discussion

Where the amplitude of vibration is smallest, in the tests with $R = 1.2$, the range of predicted values and measured values are similar, as are the mean values for each set. This suggests that the elastic model is appropriate for prediction of the foundation modulus for small-amplitude vibration. For the perpendicular-to-grain tests, the mean predicted stiffness is within 5% of the mean measured stiffness. For the parallel-to-grain tests with $R = 1.2$, the measured values are lower than predicted. The mean measured stiffness is approximately 14% lower than the mean predicted value in these tests. As noted in Section 4.1.1, for some of these tests, a steady-state value of stiffness was not achieved. The measured stiffness in each cycle continued to rise until the end of the test. It is, therefore, possible that, if the test were continued, values of steady-state stiffness closer to the predicted values might be reached.
For the greatest amplitude of load, where $R = 10$, the predicted stiffness is significantly higher than the measured stiffness in the dynamic tests both parallel- and perpendicular-to-grain. This can be explained by the reduced secant stiffness in these tests due to nonlinear behaviour at low force, as described in Section 4.1.2.

5 Conclusions

Comparison of the analytical model and the experimental results shows that, for small-amplitude vibrations and once a steady-state dynamic response has developed, an elastic orthotropic model is appropriate to estimate the dynamic stiffness of the specimen. There is considerable scatter in the measured stiffnesses between the tests, but this is reflected in the measured variation in elastic moduli. The measured stiffness is lower than predicted in the parallel-to-grain tests, and this is thought to be a result of the imperfection of the contact surface between steel and timber.
The model presents a method to relate the fundamental material properties of the timber to its behaviour as part of a connection, and this is done through a compact analytical equation. The simplicity of the calculation means that it may be applied in circumstances in which a more detailed numerical model is inappropriate, due the time or computational expense that would incur.
When the amplitude of the oscillating force was increased, even though the peak force was not increased, the specimens behaved in a more nonlinear way. This nonlinearity reduced the secant stiffness which was measured below the predicted elastic stiffness. It would seem appropriate to apply some factor in design to allow for the fact that, while an elastic analysis is appropriate for small-amplitude vibration, a reduced stiffness is expected as the amplitude of vibration increases. Definition of such a factor would require further tests with a range of amplitudes of force.
The analysis has been applied to a particular geometry in this case, in order to match a standard test method for determining the foundation modulus for a dowel-type connection in timber. In reality, the foundation modulus will depend on the geometry of the timber around the connector. Further work will seek to apply

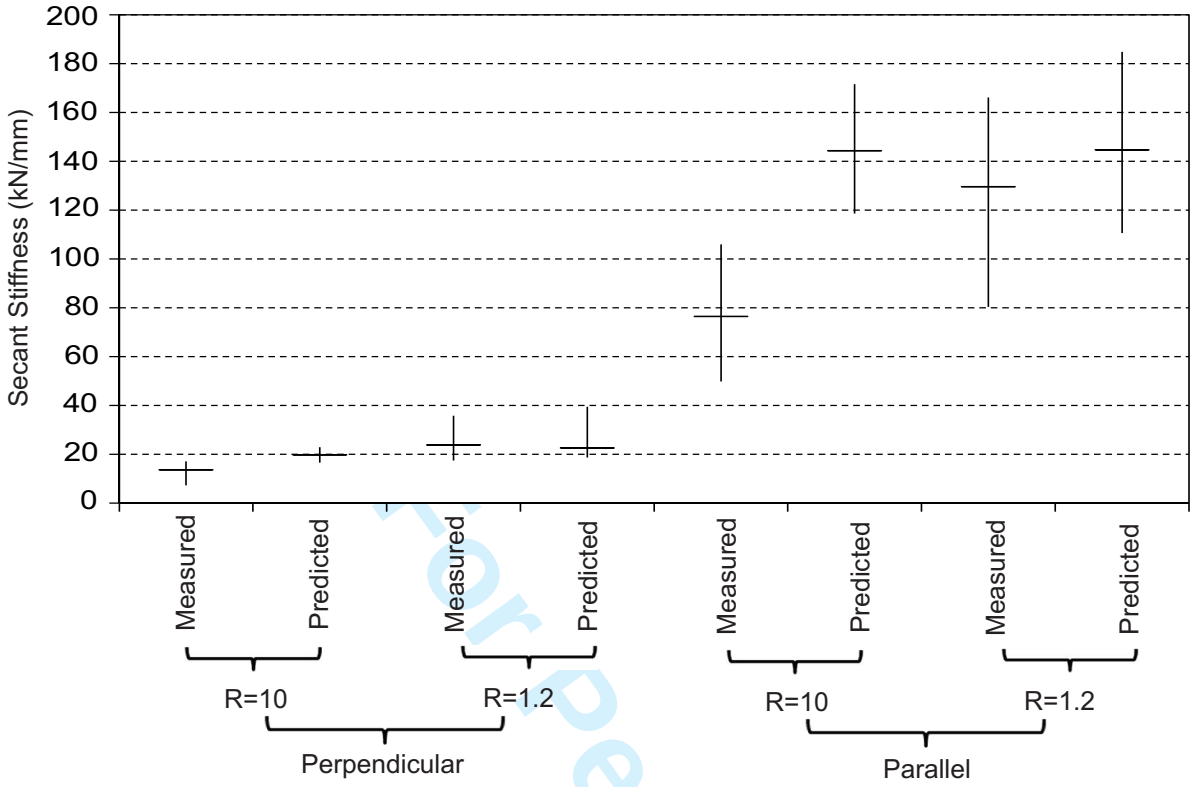

Fig. 15 Collated parallel- and perpendicular-to-grain results - The range is shown by the vertical line and the mean by the horizontal line

the analysis method to geometries which occur in real structures.

Acknowledgements Thanks to Will Bazeley and Neil Price for their help and guidance in carrying out the experimental work.

References

Allotey N, Foschi R (2004) Cyclic response of laterally loaded timber fasteners accounting for shaft friction. In: 13th World Conference on Earthquake Engineering

Aluko O, Whitworth HA (2008) Analysis of stress distribution around pin loaded holes in orthotropic plates. Compos Struct 86(4):308–313

ASTM (1997) Standard test method for evaluating dowel-bearing strength of wood and wood-based products (reapproved 2002). Tech. Rep. D5764, ASTM

Awaludin A, Hirai T, Hayashikawa T, Sasaki Y, Oikawa A (2008) Effects of pretension in bolts on hysteretic responses of moment-carrying timber joints. J Wood Sci 54(2):114–120

BSI (2002) Moisture content of a piece of sawn timber. Tech. Rep. BS EN 13183:2002, BSI

BSI (2007) Timber structures. test methods. determination of embedment strength and foundation values for dowel type fasteners. Tech. Rep. BS EN 383:2007, BSI

BSI (2009) Eurocode 5 design of timber structures. Tech. Rep. BS EN 1995-1-1:2004+A1:2008, BSI

BSI (2011) Timber structures. structural timber and glued laminated timber. determination of some physical and mechanical properties. Tech. Rep. BS EN 408:2010, BSI

De Jong T (1977) Stresses around pin-loaded holes in elastically orthotropic or isotropic plates. J Compos Mater 11(3):313

Derdas C, Kostopoulos V (2011) On the bearing failure of laminated composite pin-loaded joints: Exploitation of semi-analytical solutions for the determination of the stress state. Strain 47:320–332

Echavarra C, Haller P, Salenikovich A (2007) Analytical study of a pinloaded hole in elastic orthotropic plates. Compos Struct 79(1):107–112

Ellis BR, Bougard AJ (2001) Dynamic testing and stiffness evaluation of a six-storey timber framed building during construction. Eng Struct 23(10):1232–1242

Foliente GC (1995) Hysteresis modeling of wood joints and structural systems. J Struct Eng 121(6):1013–1022

Forest Products Laboratory (2010) Wood handbook-Wood as an engineering material. Department of Agriculture, Forest Service, Forest Products Laboratory, Madison, WI

Foschi R (2000) Modeling the hysteretic response of mechanical connections for wood structures. In: World Conference on Timber Engineering

He M (2001) Modeling three-dimensional timber light-frame buildings. J Struct Eng 127(8):901–913

Heiduschke A (2006a) Analysis of wood-composite laminated frames under dynamic loads - analytical models and model validation. part i: Connection model. Prog Struct Eng Mater 8(3):103–110

Heiduschke A (2006b) Analysis of wood-composite laminated frames under dynamic loads - analytical models and model validation. part ii: Frame model. Prog Struct Eng Mater 8(3):111–119

Heiduschke A (2008) Performance and drift levels of tall timber frame buildings under seismic and wind loads. Struct Eng Int 18(2):186–191

Hyer M, Klang E (1985) Contact stresses in pin-loaded orthotropic plates. Int J Solids Struct 21(9):957–975

Inglfsson ET, Georgakis CT, Jnsson J (2012) Pedestrian-induced lateral vibrations of footbridges: A literature review. Eng Struct 45(0):21–52

Jones RM (1975) Mech Compos Mater. Scripta Book Company, Washington D. C.

Larsen HJ, Jensen JL (2000) Influence of semi-rigidity of joints on the behaviour of timber structures. Prog Struct Eng Mater 2(3):267–277

Lekhnitskii SG (1968) Anisotropic Plates, 2nd edn. Gordon and Breach, New York

Loo WY, Quenneville P, Chouw N (2012) A numerical study of the seismic behaviour of timber shear walls with slip-friction connectors. Eng Struct 34(0):233–243

McKenzie WM, Karpovich H (1968) The frictional behaviour of wood. Wood Sci Technol 2(2):139–152

Nishiyama N, Ando N (2003) Analysis of load-slip characteristics of nailed wood joints: application of a two-dimensional geometric nonlinear analysis. J Wood Sci 49(6):505–512

Noguchi M, Komatsu K (2004) A new method for estimating stiffness and strength in bolted timber-to-timber joints and its verification by experiments (ii): bolted cross-lapped beam to column joints. J Wood Sci 50(5):391–399

Sjödin J, Enquist B, Serrano E (2006) Contact-free measurements and numerical analyses of the strain distribution in the joint area of steel-to-timber dowel joints. Eur J Wood Prod 64(6):497–506

Sjödin J, Serrano E, Enquist B (2008) An experimental and numerical study of the effect of friction in single dowel joints. Eur J Wood Prod 66(5):363–372

Šilih S, Premrov M, Kravanja S (2005) Optimum design of plane timber trusses considering joint flexibility. Eng Struct 27(1):145–154

Zhang KD, Ueng CE (1984) Stresses around a pin-loaded hole in orthotropic plates. J Compos Mater 18(5):432–446

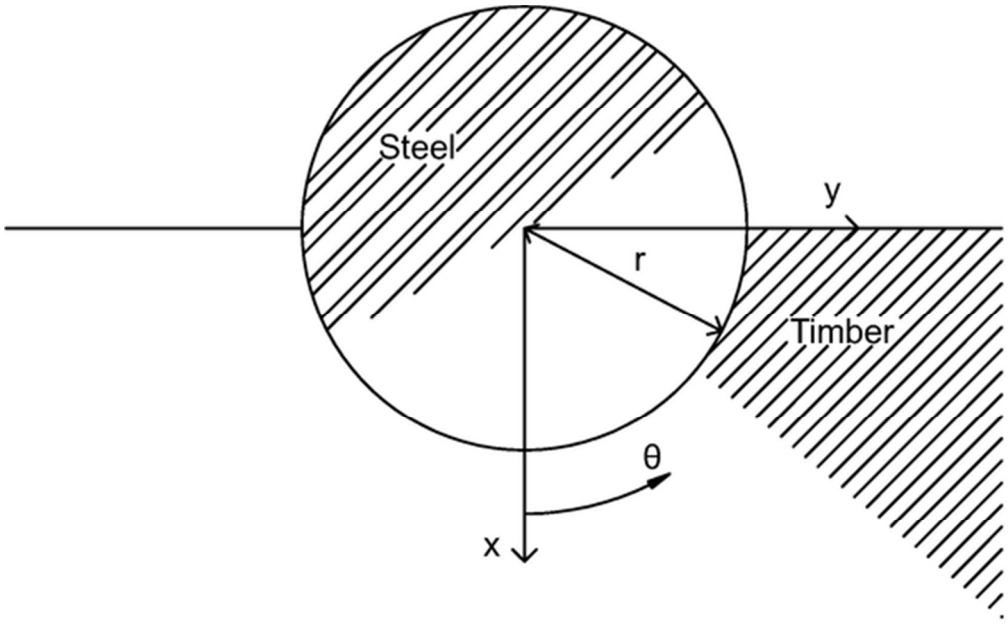

Geometry for analysis
51x31mm (300 x 300 DPI)

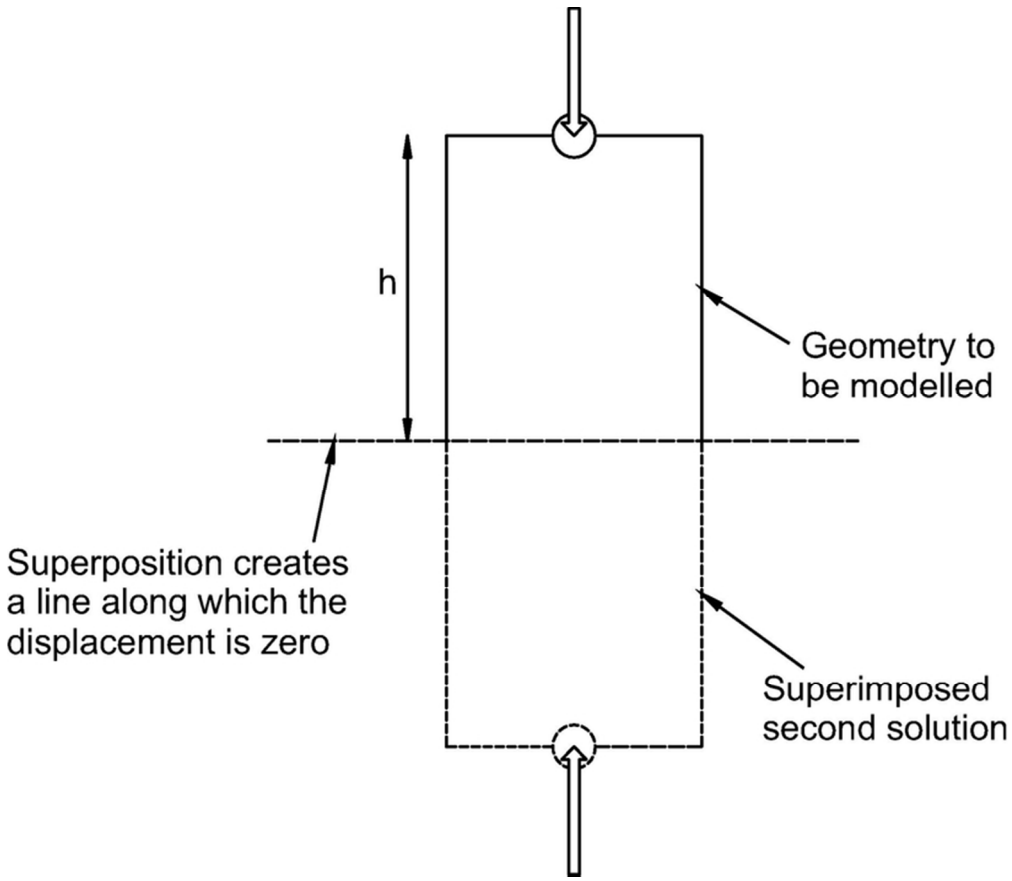

Superposition of two infinite-plate solutions to model a supported edge
69x59mm (300 x 300 DPI)

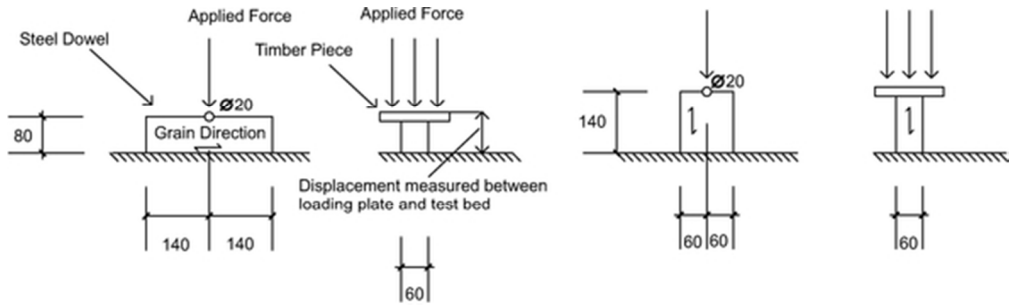

Schematic diagram of test setup with perpendicular-to-grain (left) and parallel-to-grain (right) specimens (dimensions in mm)
50x14mm (300 x 300 DPI)

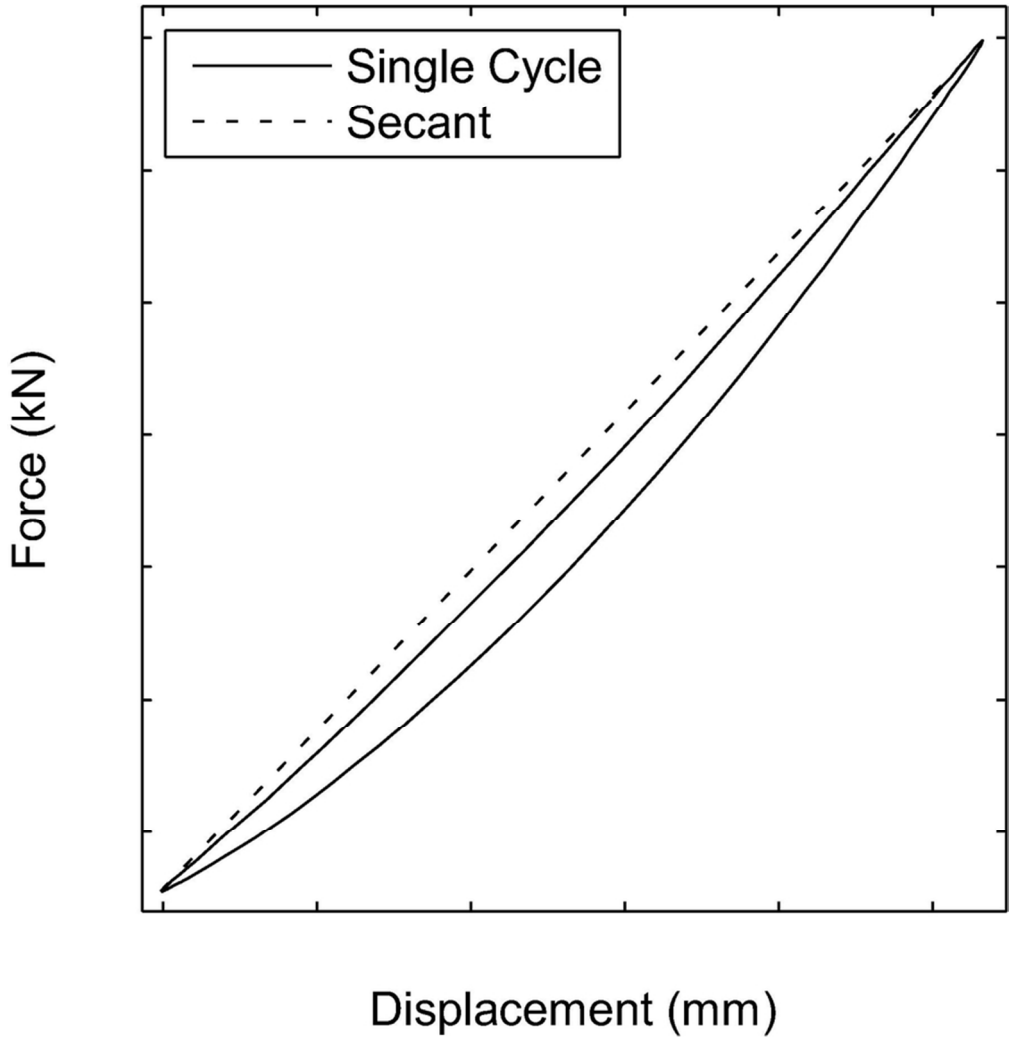

Secant stiffness
77x80mm (300 x 300 DPI)

Friction test on dynamic test specimens

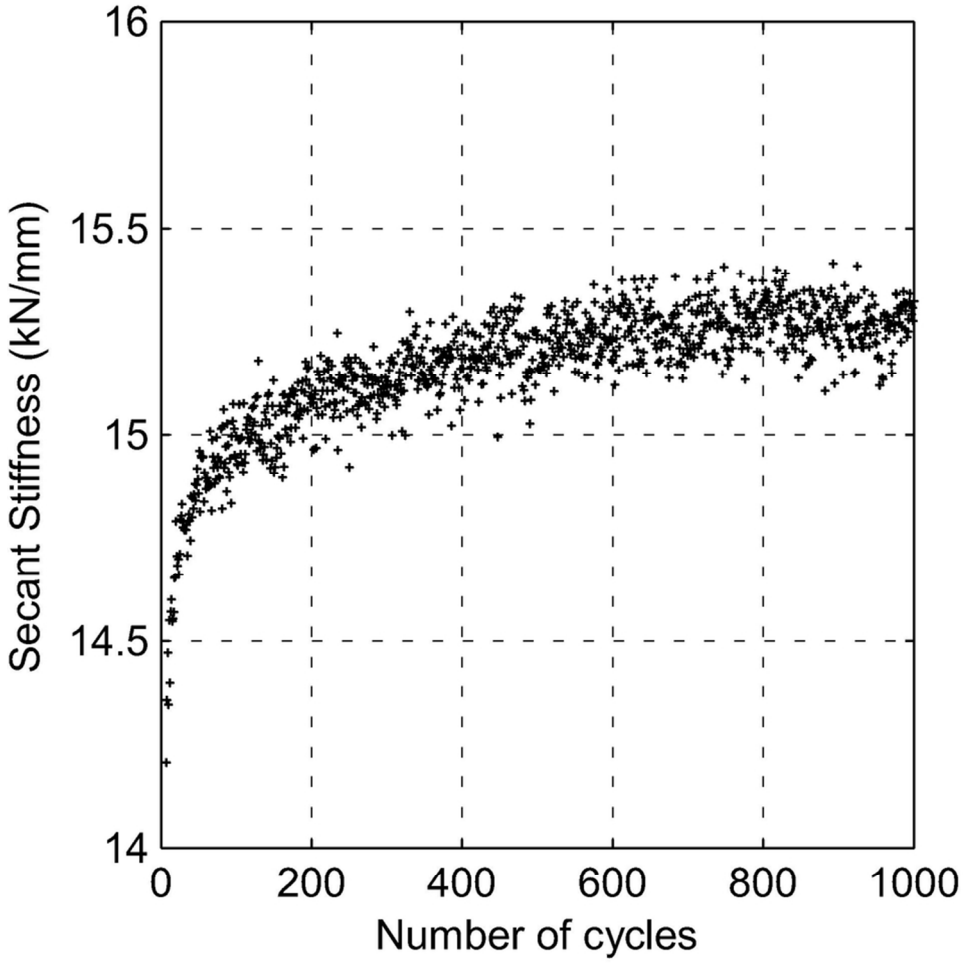

Variation of stiffness for a peak force of 40% of the embedment strength, R=10, perpendicular to grain
84x84mm (300 x 300 DPI)

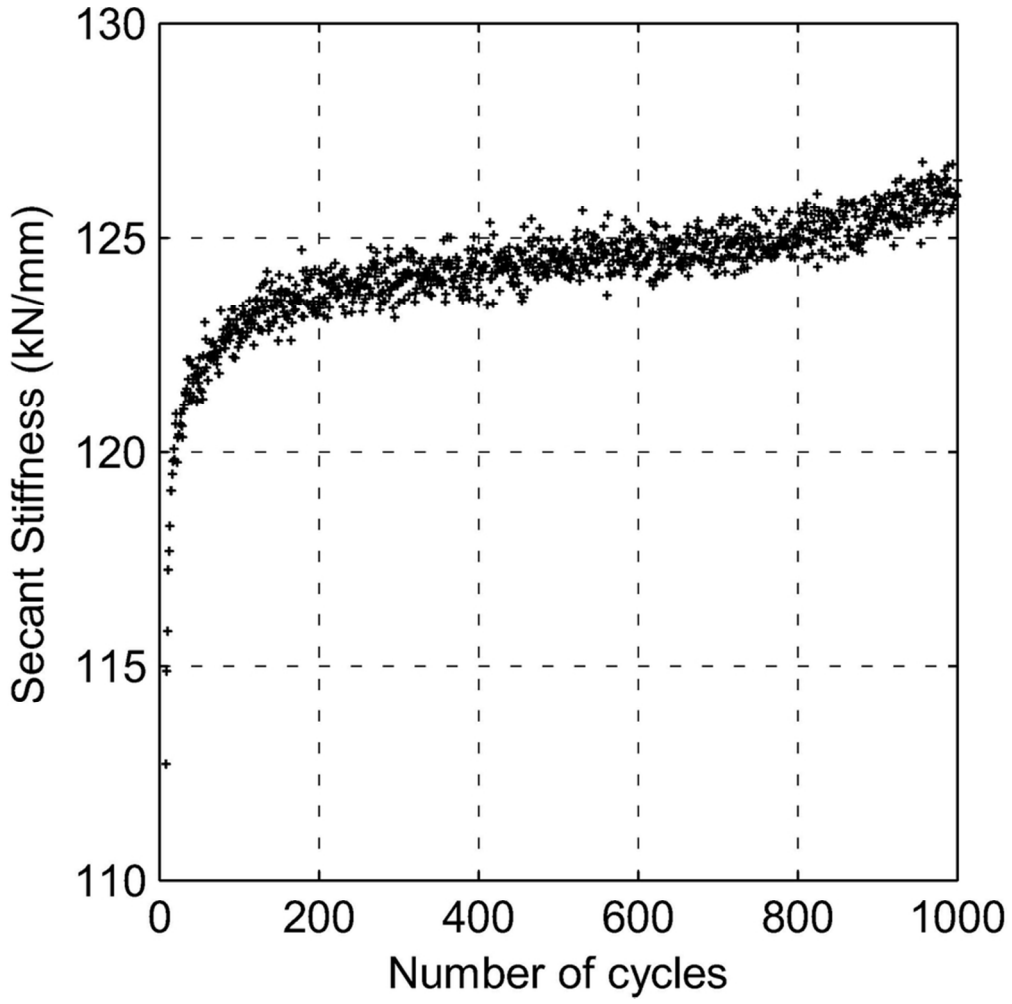

Variation of stiffness for a peak force of 40% of the embedment strength, R=1.2, parallel to grain
78x78mm (300 x 300 DPI)

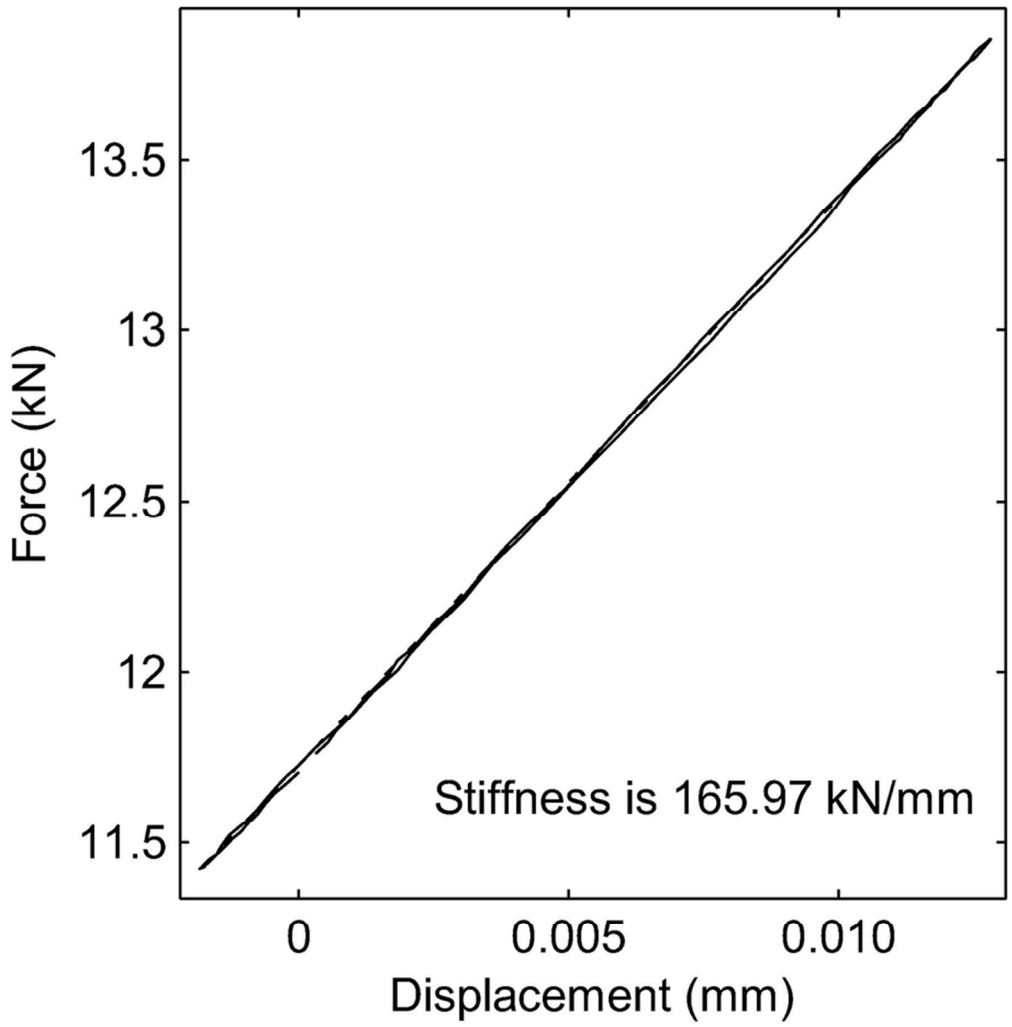

Secant stiffness for a peak force of 40% of the yield force, R=1.2
77x78mm (300 x 300 DPI)

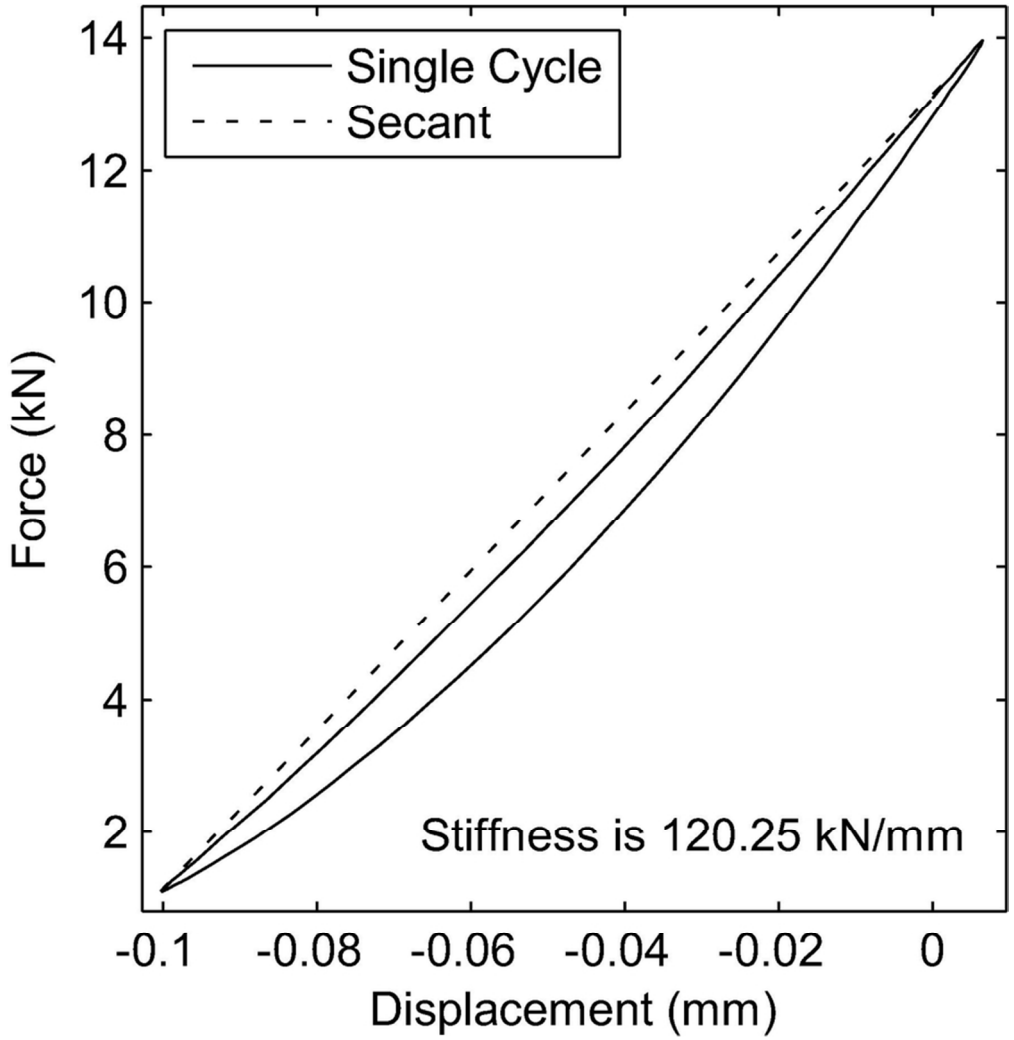

Secant stiffness for a peak force of 40% of the yield force, R=10
77x80mm (300 x 300 DPI)

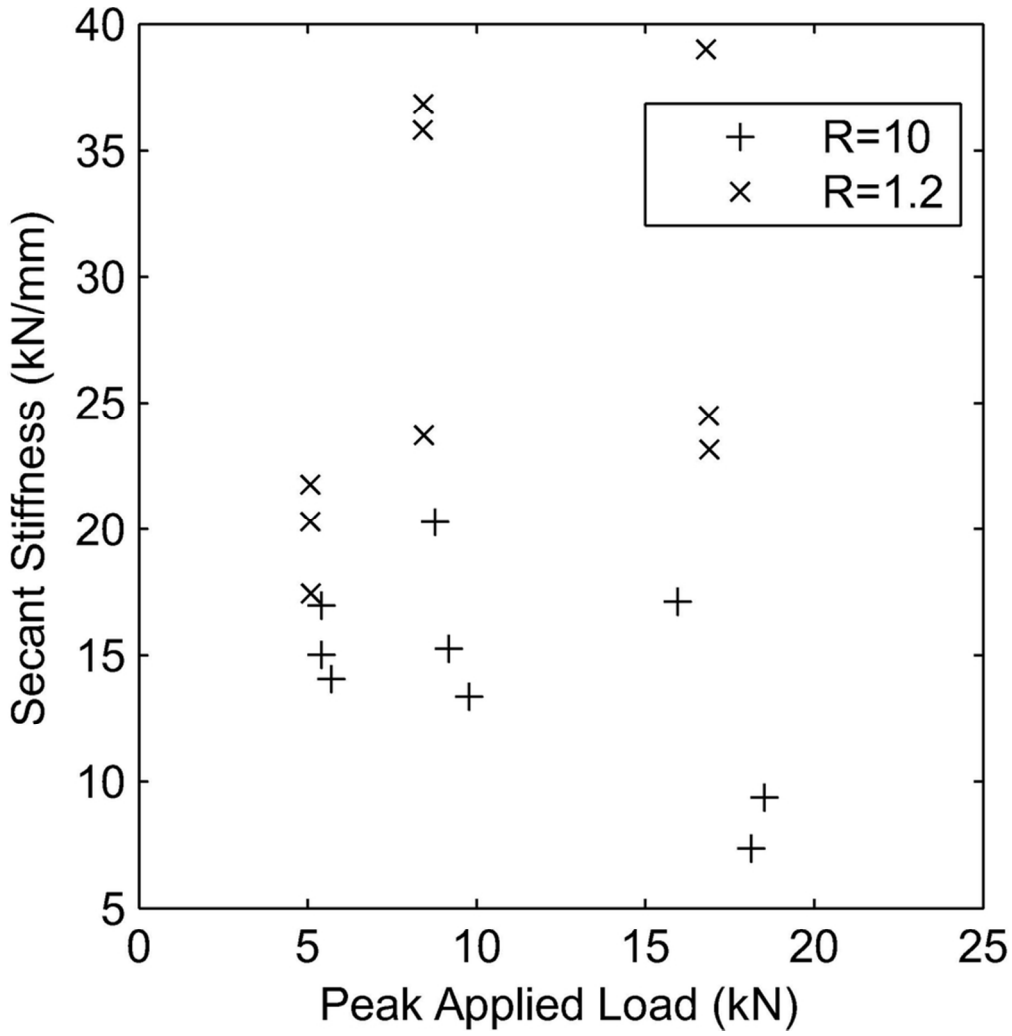

Mean secant stiffness for perpendicular to grain tests
78x80mm (300 x 300 DPI)

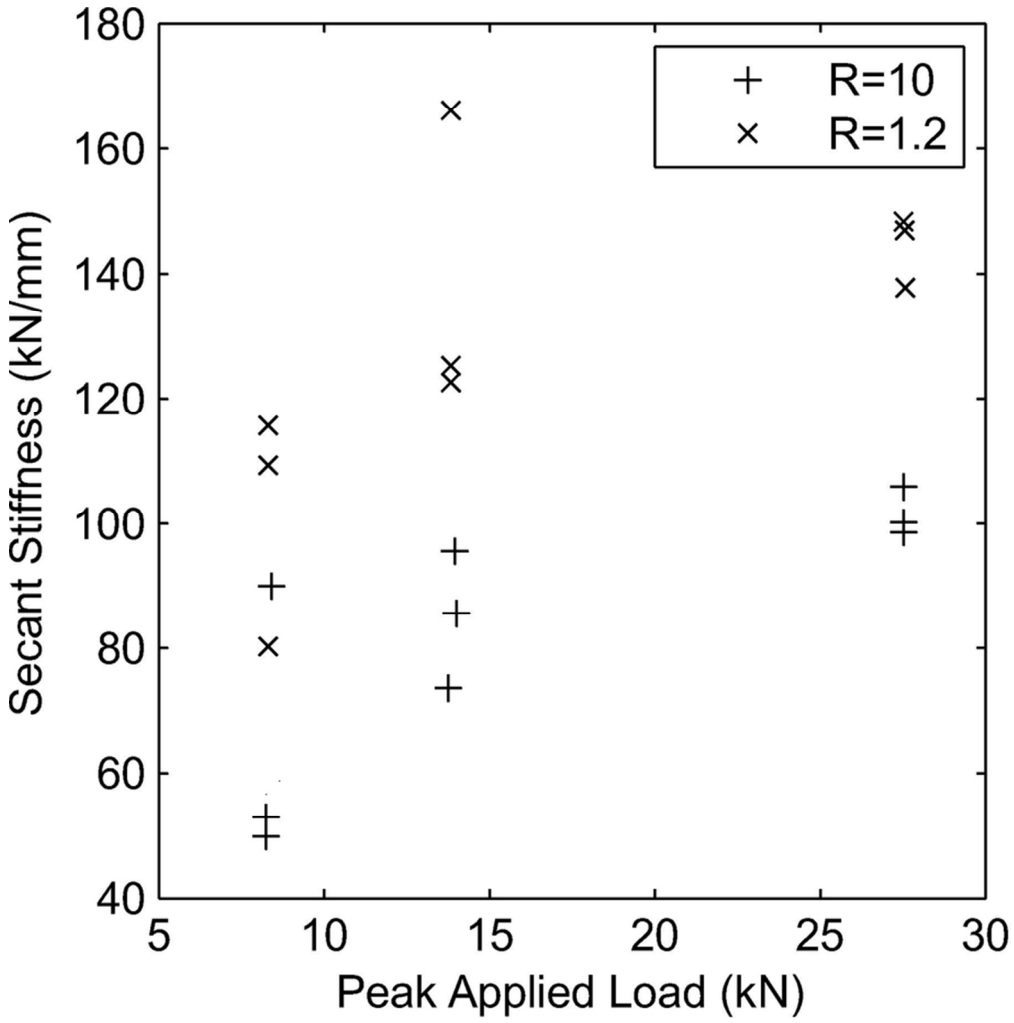

Mean secant stiffness for parallel to grain tests
77x77mm (300 x 300 DPI)

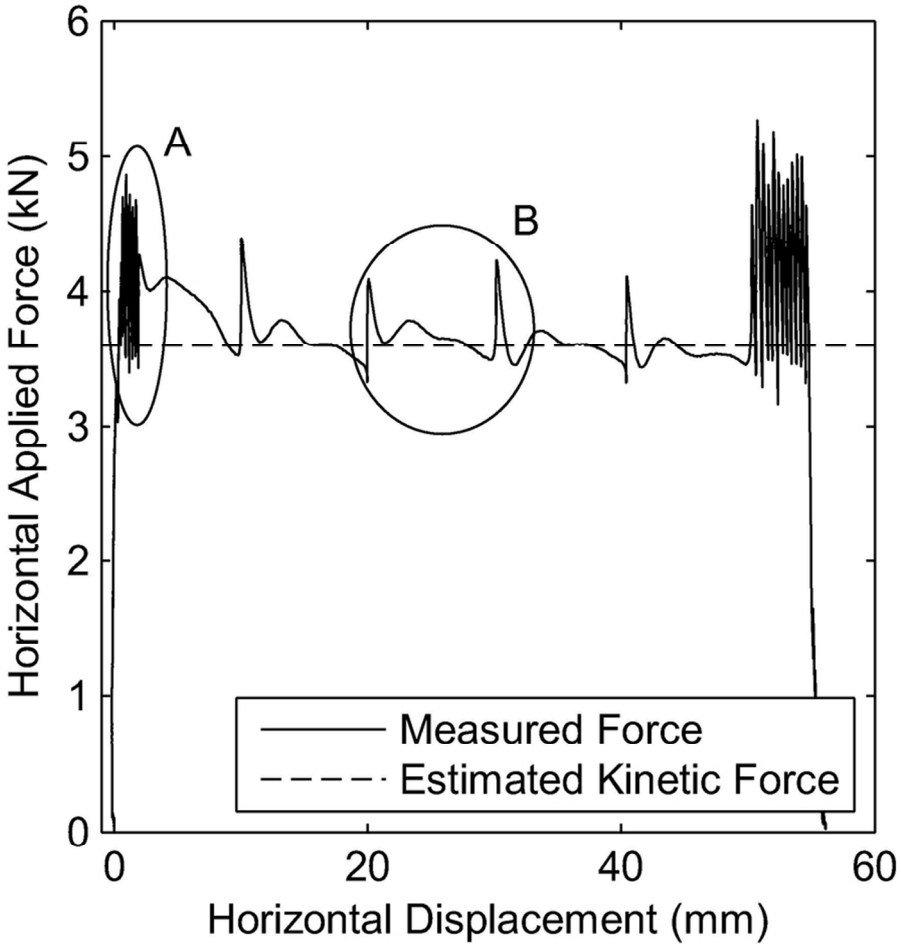

Friction test results - Specimen loaded perpendicular to the grain at 8.4kN, 40% of the predicted yield force
84x84mm (300 x 300 DPI)

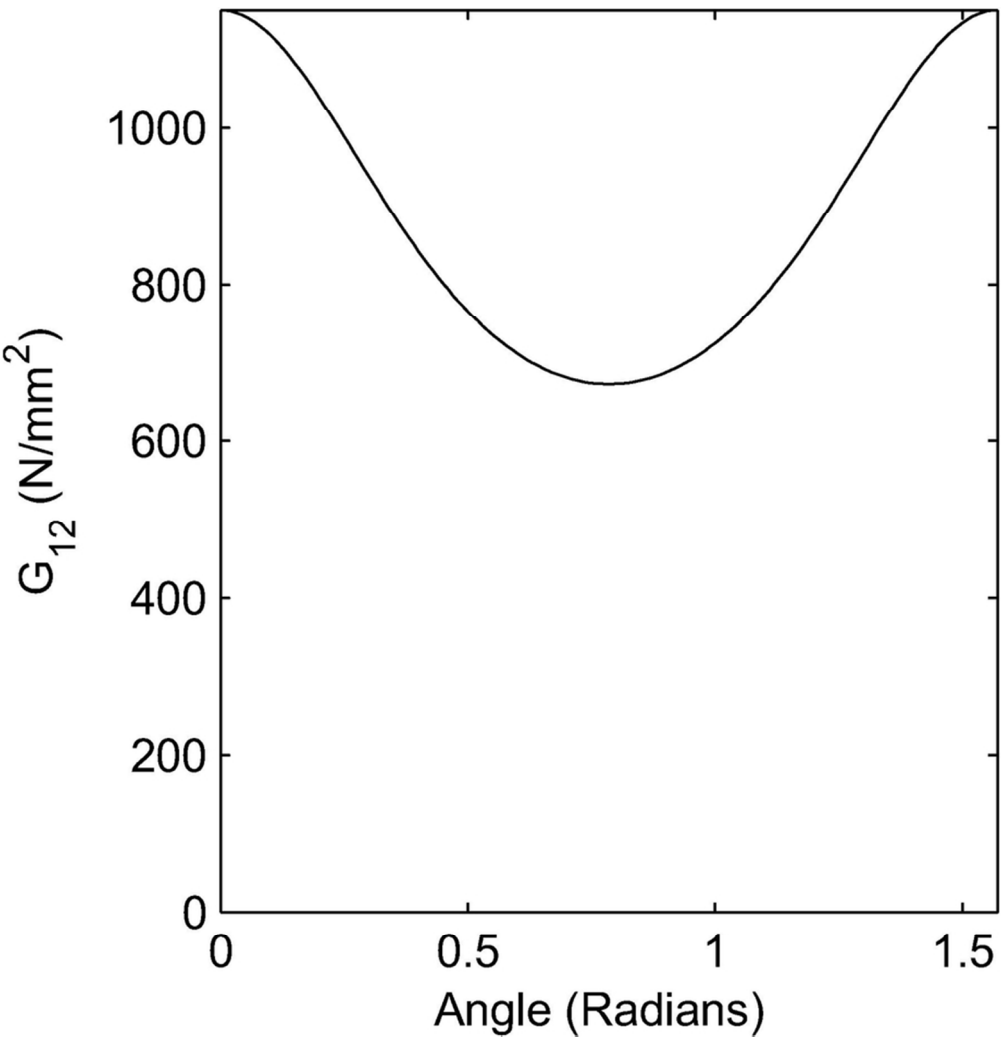

Variation of apparent shear modulus with angle from the principal direction for Douglas fir
77x80mm (300 x 300 DPI)

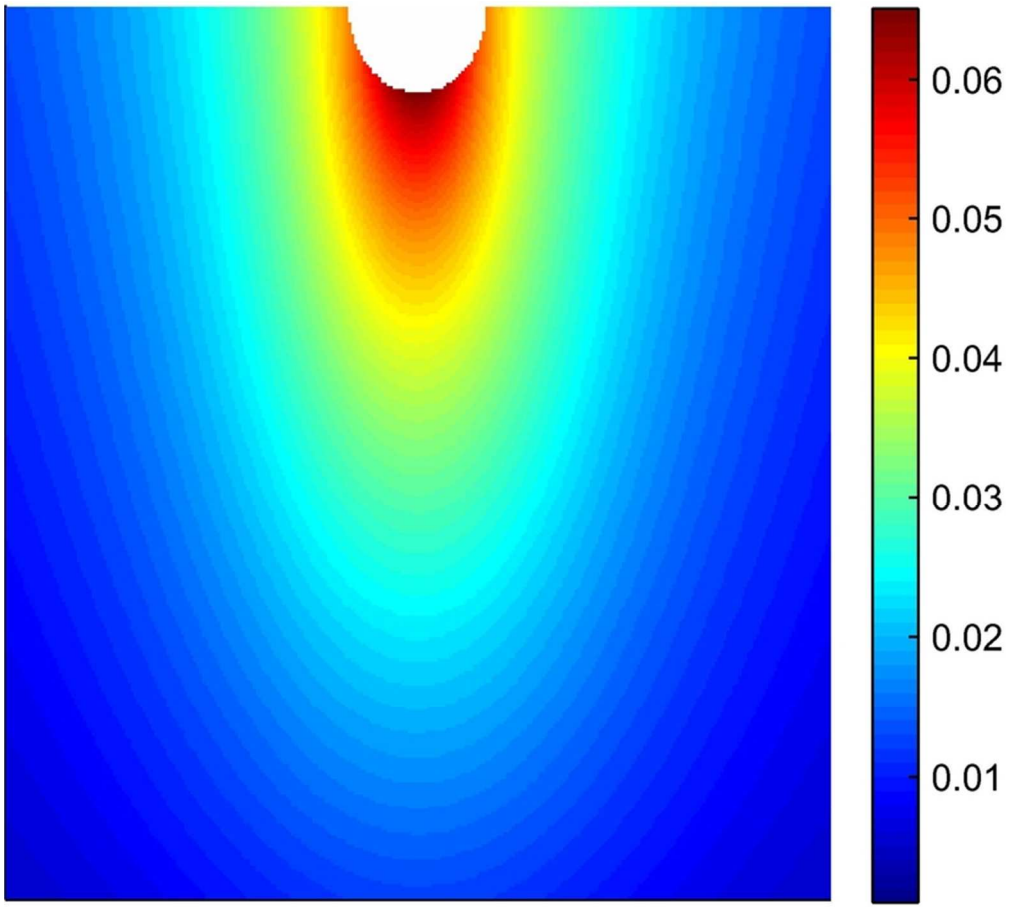

Vertical displacements in mm in the plate for a typical specimen in parallel-to-grain loading (1kN applied force)
69x62mm (300 x 300 DPI)

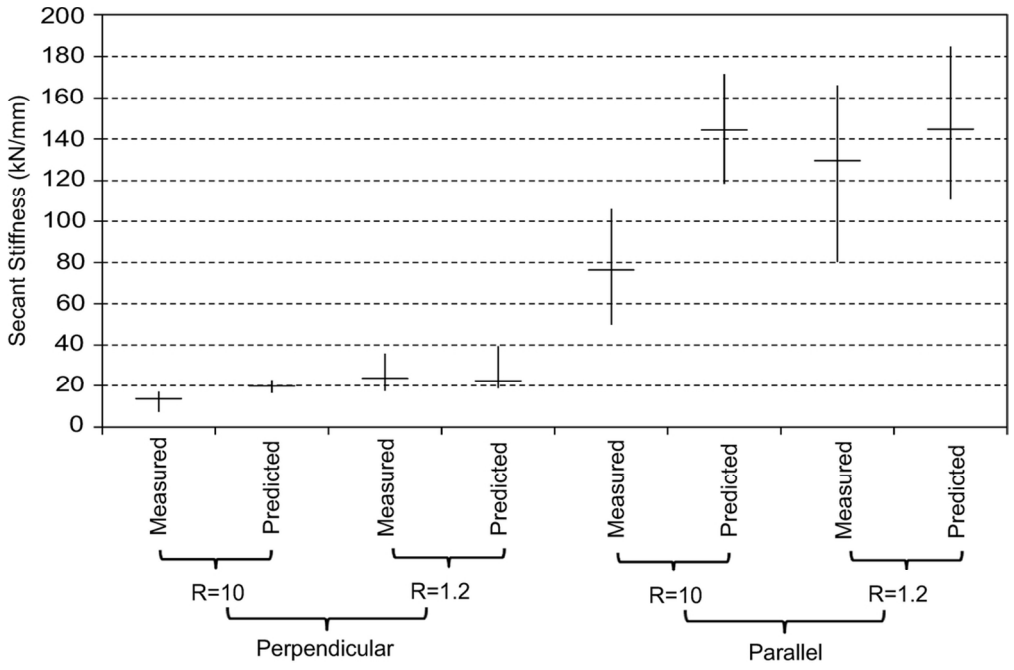

Collated parallel- and perpendicular-to-grain results - The range is shown by the vertical line and the mean by the horizontal line
103x67mm (300 x 300 DPI)